

The electronic and transport properties in the Haldane-Hubbard with odd-parity altermagnetism

Minghuan Zeng¹, Zheng Qin¹, Ling Qin², Shiping Feng^{3,4}, Dong-Hui Xu^{1,5,*} and Rui Wang^{1,5†}

¹*Institute for Structure and Function & Department of Physics & Chongqing Key Laboratory for Strongly Coupled Physics, Chongqing University, Chongqing, 400044, P. R. China*

²*College of Physics and Engineering, Chengdu Normal University, Chengdu, 611130, Sichuan, China*

³*Department of Physics, Faculty of Arts and Science, Beijing Normal University, Zhuhai, 519087, China*

⁴*School of Physics and Astronomy, Beijing Normal University, Beijing, 100875, China and*

⁵*Center of Quantum materials and devices, Chongqing University, Chongqing 400044, P. R. China*

The sublattice current is recently proposed as a feasible scheme to realize the odd-parity altermagnetism(ALM) by breaking the nonmagnetic time reversal symmetry. We first adopt the spin group method to analyze why the broken nonmagnetic time reversal symmetry(TRS) is the sufficient condition for the odd-parity ALM, and find that it is the symmetry $[\bar{C}_2||\bar{E}]$ that allows the appearance of the odd-parity ALM where \bar{C}_2 represents a 180° rotation around an axis perpendicular to the spins combined with the spin-space inversion, and \bar{E} is the inversion in real space. As a representative example with the presence of sublattice currents, the optical conductivity of Haldane-Hubbard model is further studied using the Kubo formula. It is shown that there is no spin-polarized electrical current in both the longitudinal and traverse directions because of TRS in the odd-parity ALM, and they display a significant peak in the vicinity of the single-particle direct energy gap which reflects that both the longitudinal and traverse optical conductivities are dominated by the quasiparticle excitations around the Dirac points. We also study the hole doping dependence of the anomalous Hall conductivity σ_{Hall} as well as the staggered magnetization M , and find that they display opposite behaviors, i.e., σ_{Hall} in the ALM CI state is diminished monotonically from its initial value $C = 2$ at half-filling as the hole doping is increased, while in the ALMI state exhibits a non-monotonous behavior.

PACS numbers: 74.62.Dh, 74.62.Yb, 74.25.Jb, 71.72.-h

Introduction.—Recent series of theoretical and experimental reports^{1–18} have driven attention to time-reversal symmetry-breaking spintronic and spin-splitting phenomena in materials with collinear-compensated magnetic order incompatible with conventional ferromagnetism(FM) or antiferromagnetism(AFM). The alternating spin polarizations in both the real-space crystal structure and the momentum-space band structure characteristic of this unconventional magnetic phase suggest a term altermagnetism(ALM). By employing and developing the spin-group formalism^{19–21} of symmetry transformations in the decoupled real and spin space, three distinct phases of non-relativistic collinear magnetism are derived^{22–24}. The first phase has single spin lattice (or opposite-spin sublattices not connected by any symmetry transformation). It corresponds to conventional ferromagnetism²⁵. The second phase has opposite-spin sublattices connected by translation or inversion (or both), and corresponds to conventional antiferromagnetism^{19,26,27}. The third phase has opposite-spin sublattices connected by rotation (proper or improper and symmorphic or nonsymmorphic) but not connected by translation or inversion. Unlike the conventional ferromagnetic phase with a nonrelativistic magnetization and spin-split bands that break time-reversal symmetry²⁵(TRS), and unlike the conventional antiferromagnetic phase with nonrelativistic spin-degenerate time-reversal invariant bands and zero net magnetization^{26,28–30}, the third

phase has split but equally populated up- and down-spin energy dispersions in the band structure that break TRS. Furthermore, principles based on the spin-group symmetries guide researchers to find rich materials having the third phase with an extraordinary microscopic spin-splitting mechanism, whose energy scale and momentum dependence are determined by the anisotropic electric crystal potential, i.e., by the scale and momentum dependence of the band splitting of the nonmagnetic phase^{16–18,22,23}.

However, in previous works, nonmagnetic crystal structures are assumed time-reversal-symmetric, which naturally leads to that altermagnetism induced by the anisotropic electric crystal potential is of even parity^{22–24}. Then a question arises, can the ALM of odd parity be reached if the nonmagnetic TRS is broken by introducing the sublattice currents or light? There have been several works proving that the above elements are efficient to induce the odd-parity altermagnetism³¹, while there lacks a systematic investigation based on the spin-group formalism^{19–21} of symmetry in the decoupled real and spin space to illustrate the relation between the broken TRS in the nonmagnetic phase and the appearance of the odd-parity ALM. In addition, up to now, the transport properties of the odd-parity ALM system have not been investigated so far.

As a representative example, Haldane-Hubbard model breaks its nonmagnetic TRS via sublattice currents induced by the alternating magnetic flux in real space.

Though previous works for its phase diagram versus the Haldane hopping λ and electron onsite coulomb repulsive interaction U uncovered compensated collinear magnetism by using multiple theoretical techniques^{32–38}, this compensated collinear magnetism was inaccurately classified as AFM³¹. Until very recently, Lin restudied this theoretical model³¹ within the HF approximation where opposite-spin segments in real and momentum space are connected by the transformation $[C_2||C_6^1]$ that represents a rotation of $\frac{\pi}{6}$ in real space, followed by a 180° rotation around an axis perpendicular to the spins. This new phase is then reclassified as the odd-parity ALM of f wave and proved that the sublattice current is an efficient way for the realization of odd-parity ALM by breaking the TRS in the nonmagnetic phase.

In this Letter, we first adopt the spin group method^{19–21} to study the relationship between the odd-parity ALM and the broken TRS in the nonmagnetic state. It is shown that compared to the symmetry $[\bar{C}_2||T]$ in even-parity ALM systems where \bar{C}_2 is a 180° rotation around an axis perpendicular to the spins combined with the spin-space inversion in the spin-only group, and T represents the time reversal transformation, the symmetry connected to \bar{C}_2 now changes into the form: $[\bar{C}_2||\bar{E}]$ with \bar{E} being the spatial inversion, implying that for the odd-parity ALM, the single-particle energy dispersion is subjected to the relation $E_{\mathbf{k}\sigma} = E_{-\mathbf{k}-\sigma}$. As a representative example in the presence of sublattice currents, the transport properties of Haldane-Hubbard model is further studied using the Kubo formula. It is shown that both the longitudinal and traverse optical conductivities are not spin-polarized, and display a significant peak in the vicinity of the single-particle direct energy gap, reflecting that both of them are dominated by the quasiparticle excitations in the vicinity of Dirac points. We also study the hole doping dependence of the anomalous Hall conductivity σ_{Hall} as well as the staggered magnetization M . The results show that they display opposite behaviors, i.e., σ_{Hall} in the ALM CI state is diminished monotonically from its initial value $C = 2$ at half-filling as the hole doping is increased, while that in the ALMI state exhibits a non-monotonous behavior which is similar to the interacting modified Kane-Mele model³⁹.

Symmetry analysis and the theoretical model.—In general, spin groups can be factorized as a direct product $\mathbf{r}_s \times \mathbf{R}_s$ of the spin-only group \mathbf{r}_s containing transformations in the spin space alone, and the nontrivial spin groups \mathbf{R}_s containing the elements $[R_i||R_j]$ ^{20–22}. For the collinear spin arrangements on crystals, the spin-only group is given by $\mathbf{r}_s = \{C_\infty, \bar{C}_2 C_\infty\}$ ^{20–22}. Here C_∞ is a group consisting of all rotations around the common axis of spins in the spin space. The rotation symmetry C_∞ enables spin a good quantum number with a common quantization axis in momentum space across the nonrelativistic band structure. The electronic structure is thus strictly separated into nonmixing up- and down-spin channels.

The symmetry \bar{C}_2 in the spin-only group implies a symmetry of $[\bar{C}_2||\bar{E}]$ or $[\bar{C}_2||\bar{E}t]$ in the collinear magnets where TRS is broken in the nonmagnetic phase induced by sublattice currents or light³¹ with t being the spatial translation. When applying the transformation $[\bar{C}_2||\bar{E}]$ on spin (σ) and crystal-momentum (\mathbf{k})-dependent bands $E_{\mathbf{k}\sigma}$, we obtain $[\bar{C}_2||\bar{E}]E_{\mathbf{k}\sigma} = E_{-\mathbf{k}-\sigma}$, and because $[\bar{C}_2||\bar{E}]$ is a symmetry of the system, we have $E_{\mathbf{k}\sigma} = E_{-\mathbf{k}-\sigma}$, which indicates that TRS is present in the odd-parity ALM materials.

For an ALM material, opposite-spin sublattices can not be connected by time reversal transformation combined with real-space inversion or the spatial translation, while is connected by the transformation $[C_2||C_n^1]$ where C_2 is a 180° rotation around an axis perpendicular to the spins and C_n^1 represents the real-space rotation symmetry in the nonmagnetic phase with n being the order of rotation axis. In this sense, the symmetry transformation $[C_2||C_n^1]^m$ with m being the odd or even number connects the opposite- and same-spin sublattice, respectively. Then acting $[C_2||C_n^1]^{n/2}$ on the spin- and momentum-dependent bands $E_{\mathbf{k}\sigma}$ gives rise to

$$[C_2||C_n^1]^{n/2}E_{\mathbf{k}\sigma} = \begin{cases} E_{-\mathbf{k}\sigma}, & , n/2 \text{ is even} \\ E_{-\mathbf{k}-\sigma}, & , n/2 \text{ is odd} \end{cases} \quad (1)$$

Haldane-Hubbard model.—As a representative example with the presence of sublattice currents that break TRS in the nonmagnetic phase, the Haldane-Hubbard model⁴⁰ is studied:

$$\begin{aligned} H = & -t \sum_{\langle ij \rangle} [C_{iA}^\dagger C_{jB} + \text{H.C.} + \mu \delta_{ij} \sum_s C_{is}^\dagger C_{js}] \\ & + \lambda \sum_{s=A,B} \sum_{\langle\langle ij \rangle\rangle} C_{is}^\dagger e^{i\frac{\pi}{2}\nu_{ij}} C_{js} + U \sum_{i,s=A,B} n_{is\uparrow} n_{is\downarrow} \end{aligned} \quad (2)$$

where $\langle ij \rangle$ and $\langle\langle ij \rangle\rangle$ denote that the summation is over all the nearest and next nearest neighbor sites, respectively; $C_{is}^\dagger = (C_{is\uparrow}^\dagger, C_{is\downarrow}^\dagger)$ is a two-component spinor with $s = A, B$ denoting two sublattices; $\nu_{ij} = \pm 1$ is the Haldane phase factor for clockwise and anticlockwise path connecting the next nearest neighbor sites i and j ; $n_{is\sigma} = C_{is\sigma}^\dagger C_{is\sigma}$ is the electron occupation number operator at site is with spin σ . The detailed lattice set-up in real and momentum space is provided in Sec. I of the Supplemental material. In the following, the nearest neighbor hopping integral t and the lattice constant a have been set as the energy and length unit, respectively.

The above Hamiltonian is solved within the Hartree-Fock approximation with the mean-field parameters:

$$n = \frac{1}{2N} \sum_{is\sigma} \langle C_{is\sigma}^\dagger C_{is\sigma} \rangle, \quad (3a)$$

$$M = \frac{1}{2N} \sum_{is} (-1)^s [\langle C_{is\uparrow}^\dagger C_{is\uparrow} \rangle - \langle C_{is\downarrow}^\dagger C_{is\downarrow} \rangle], \quad (3b)$$

where $s = 0, 1$ is for sublattice A and B, respectively, and N is the number of unit cells in the system. The detailed derivation is provided in Sec. IIA of the supplemental material. In this work, the chemical potential μ and the staggered magnetization M are self-consistently determined at any given parameters λ and U , as well as the hole doping concentration δ . Moreover, if not specified, the system is set to be half-filled with $n = 1 - \delta = 1$, where the particle-hole symmetry requires that $\mu = -U/2$.

Electronic states and phase diagram.— To establish the ALM characteristics in Haldane-Hubbard model, we first study the curves of constant energy (CCE) for up- and down-spin electron quasiparticles via the electron spectral function $A_\sigma(\mathbf{k}, \omega) = -2\text{Im}G_\sigma(\mathbf{k}, \omega + i\Gamma)$ at $\lambda = 0.3$ and $U = 4.8$ with $\omega = 1$ and 2 in Fig.1 (a) and (b), respectively. The major characteristics are summarized as: (i) the electron spectrum function exhibits prominent $[C_2][C_6^1]$ symmetry with $E_{\mathbf{k}\sigma} = E_{-\mathbf{k}-\sigma}$ which is required by the odd-parity ALM as shown in Eq.(1); (ii) at low energies, the CCE's for up- and down-spin electrons are centered around the Dirac points K' and K , respectively, and do not intersect with each other which enables us to recognize the odd-parity ALM via the quasiparticle scattering interference (QSI) spectrum easily because the QSI spectrum is closely associated with the contour of CCE's of the single-particle energy dispersion^{41,42}, while those at higher energies such as $\omega = 2$ intersect with each other and makes its QSI spectrum complicated and may not become an experimentally feasible measurement for identifying the odd-parity ALM. In addition, the TRS in odd-parity ALM systems indicates that we have more methods to alter its physical properties such as the sublattice potential, light, and magnetic impurities. Here by including the sublattice potential V , the single-particle energy gap in Eq.(7) of the supplemental material becomes $\Delta_{\mathbf{k}\sigma} = V - UM\sigma + 2\lambda\gamma_{2\mathbf{k}}$, then leads to that $E_{\mathbf{k}\sigma} \neq E_{-\mathbf{k}-\sigma}$, indicating that the TRS is no longer existent in the presence of sublattice potential.

At half-filling, after self-consistently determining the staggered magnetization M through the second equation in Eq.(3) as well as calculating the Thouless-Kohmoto-Nightingale-Nijs (TKNN) number, the phase diagram versus the Haldane hopping λ and electron onsite coulomb repulsive interaction strength U is plotted in Fig.1(c). It is worth mentioning that although the similar phase diagram has been obtained in previous works^{32-35,37,38}, the ALM insulating state was classified inaccurately as an AFM insulating state³¹. The main characteristics in Fig.1(c) can be summarized as: (i) the competition between the alternate magnetic flux induced by the Haldane term and the staggered magnetization coming from the electron onsite coulomb repulsive interaction leads to that for the growing Haldane hopping strength λ , the critical interaction strength for the transition from the nonmagnetic Chern insulating state to the magnetic state increases monotonously; (ii) for all Haldane hopping strengths, as the staggered

magnetization sets in, the sublattice currents induced by the alternate magnetic flux from the Haldane term transit the traditional AFM insulating phase into the ALM insulating state³¹; (iii) for large Haldane hopping strengths, in the intermediate interaction regime in grey color, the ALM insulator coexists with Chern insulator with $C = 2$, and thus this state is renamed as ALM Chern insulator.

To further study the topological phase transition for large λ 's, we investigate the single-particle energy gap $\Delta_{\mathbf{k}\sigma}$ in Eq.(7) of the supplemental material as a function of momentum along the zigzag direction in Fig.1(d) with $\lambda = 0.3$ as well as $U = 4.65$ (black), 4.75 (red), 4.85 (blue), and 4.95 (magenta). Here $\Delta_{\mathbf{k}\sigma}$ for up- and down-spin electron quasiparticles are plotted by solid and dashed lines, respectively. The main characteristics of this figure can be described as: (i) the Haldane hopping opens opposite energy gaps at two Dirac points: K and K' ; (ii) for up-spin electrons, the energy gap at K is strengthened monotonously as the interaction strength U increases, while that at K' is first diminished until vanishes, and then increases monotonically as U is further enhanced, while the opposite applies for down-spin electrons. To sum up, for the spinful Haldane-Hubbard model with large λ 's, the Haldane hopping first opens opposite energy gaps at Dirac points K and K' , and drives the system into the topologically nontrivial state with $C = 2$, while as the staggered magnetization sets in with small energy gap component $-\sigma UM$, the sign of the energy gap at K and K' are still opposite and the system remains a Chern insulator with $C = 2$. However, as U further increases with the magnetic component of the energy gap overwhelming that opened by the Haldane hopping, the energy gaps at K and K' are negative and positive for up- and down-spin electrons, respectively, and the system transits into the topologically trivial ALM insulating state. We note that though the energy gap in the Haldane-Hubbard model has been discussed before^{32,33,35,37}, while this is the first time that a momentum-dependent single-particle energy gap is directly derived from the electron quasiparticle energy dispersion [See Eq.(7) in the supplemental material].

Optical conductivities and the anomalous Hall conductivity—The optical conductivity is closely associated with the electron propagator in momentum space

$$\tilde{G}_\sigma(\mathbf{k}, i\omega)^{-1} = i\omega - H_{\mathbf{k}\sigma}, \quad (4)$$

where $i\omega = i(2n + 1)\pi/\beta$ is the fermionic Matsubara frequency with n being integers and β being the inverse of temperature, as well as $H_{\mathbf{k}\sigma}$ represents the Hamiltonian in momentum space [See Eq.(6) in Sup. Mat.]. The linear response theory allows one to reach the optical conductivity in terms of the Kubo formula⁴³

$$\sigma_{ij}(\Omega, T) = -\frac{\text{Im}\Pi_{ij}(\Omega)}{\Omega}, \quad (5)$$

where $\Pi_{ij}(\Omega)$ is the retarded electron current-current

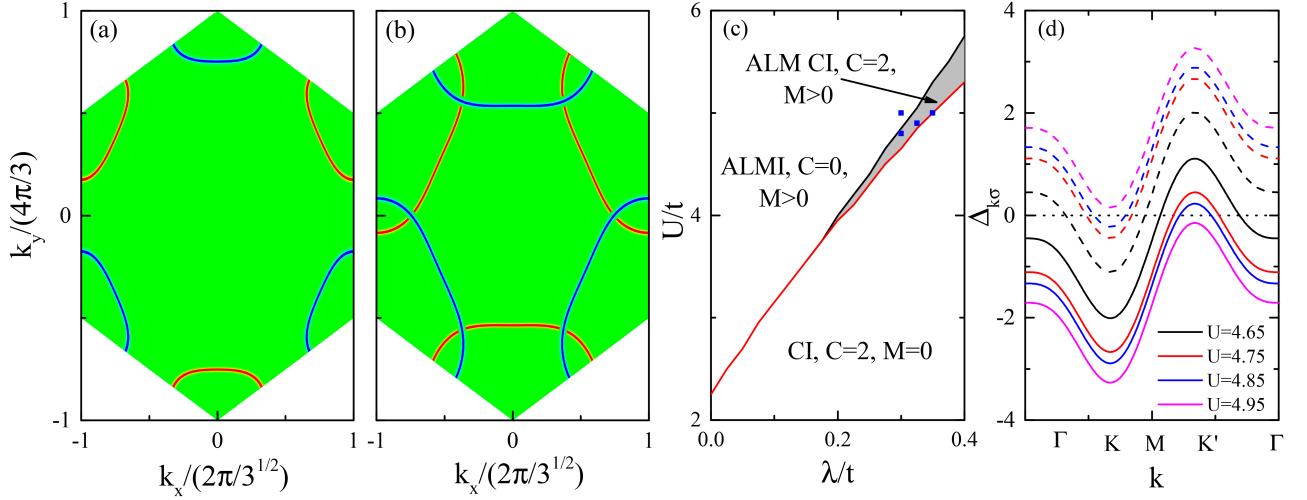


FIG. 1. (Color online) The electron spectrum function $A_\sigma(\mathbf{k}, \omega)$ as a function of momentum at $\lambda = 0.3$ and $U = 4.8$ in the reduced first Brillouin zone with $\omega = 1$ (a) and 2 (b), respectively, where the CCE for up- and down-spin electrons are plotted in red and blue color, respectively; (c) The phase diagram of the half-filled Haldane-Hubbard model as a function of Haldane hopping strength λ and electron onsite coulomb repulsive interaction strength U , which is composed of three regimes: Chern insulator(CI) with the TKNN number $C = 2$ at small U 's, the odd-parity ALM Chern insulator(ALM CI) with $C = 2$ and nonzero staggered magnetization for intermediate interaction strengths, and odd-parity ALM insulator(ALMI) in the strong interaction regimes. (d) The momentum dependence of the energy gap function $\Delta_{k\sigma}$ along the zigzag direction in the first Brillouin zone[See Fig.1 in the supplemental material] with $\lambda = 0.3$ as well as $U = 4.65$ (black), 4.75 (red), 4.85 (blue), and 4.95 (magenta), where the energy gap function for up- and down-spin electron quasiparticles are represented by solid and dashed lines, respectively.

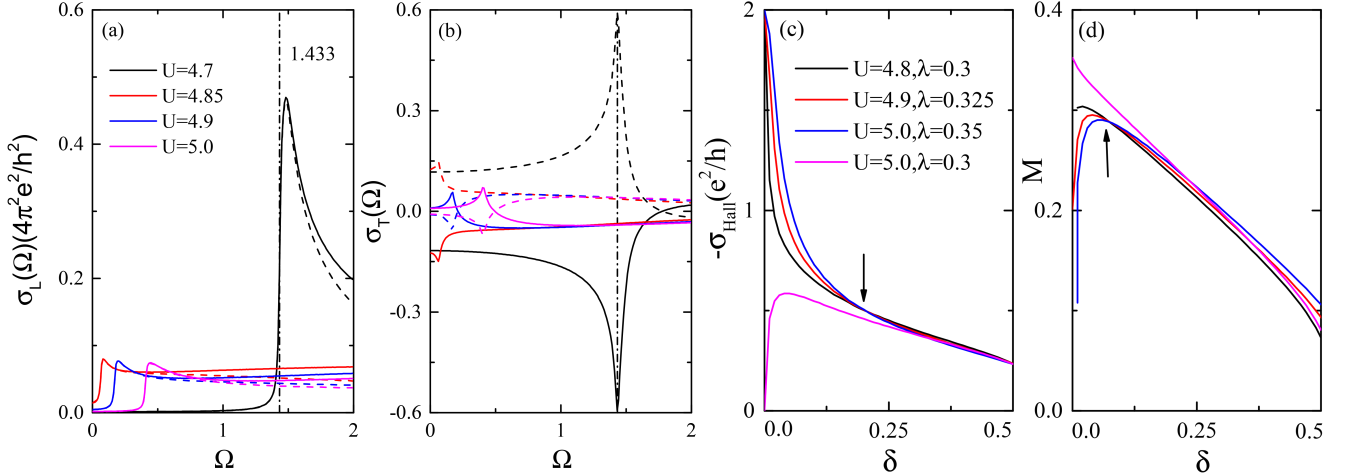


FIG. 2. (Color online) (a) The longitudinal optical conductivity σ_{xx} (solid lines) and σ_{yy} (dashed lines) as a function of energy Ω at $\delta = 0$ and $\lambda = 0.3$ with $U = 4.7$ (black), 4.85 (red), 4.9 (blue), and 5.0 (magenta); (b) The corresponding traverse optical conductivity σ_{xy} (solid lines) and σ_{yx} (dashed lines). The black dot dashed lines in this figure denote the single-particle direct energy gap $2|\Delta_{-1\uparrow}|$ [See Eq.(6)] at $\lambda = 0.3$ and $U = 4.7$; (c) Anomalous Hall conductivity σ_{Hall} and (d) the staggered magnetization M as a function of hole doping concentration δ for $U = 4.8$ and $\lambda = 0.3$ (black), $U = 4.9$ and $\lambda = 0.325$ (red), $U = 5.0$ and $\lambda = 0.35$ (blue), as well as $U = 5.0$ and $\lambda = 0.3$ (magenta). The above parameters have been denoted by blue squares in Fig.1(c)

correlation function with i, j being x and y , respectively, the derivation of which in the Matsubara representation is presented in Sec. IIB of the supplemental material.

The significant spin splitting in the CCE's of electron quasiparticles has been proved not a sufficient condition

for the occurrence of spin current⁴⁴, thus it is natural to ask whether the spin-polarized electrical current can be realized in odd-parity ALM materials. Before discussing the transport properties, we first expand the electron quasiparticle energy dispersion[See Eq.(7) in the

supplemental material] around the Dirac points K and K'. In the vicinity of K and K' with $\mathbf{k} = K^{(\prime)} + \mathbf{q}$, the momentum-dependent function $\gamma_{1/2\mathbf{k}}$ in the Sup. Mat. can be linearized as $\gamma_{1\mathbf{q}} = -s\frac{3\sqrt{3}}{2} + 0(q^2)$ and $\gamma_{2\mathbf{q}} = \frac{\sqrt{3}}{2}(iq_x - sq_y) + 0(q^2)$ with $s = \pm 1$ for valley K and K', respectively. Therefore the energy dispersion of electron quasiparticles at around the Dirac points can be linearized as

$$E_{q s \sigma}^{(\pm)} \approx \mu + \frac{nU}{2} \pm |\Delta_{s\sigma}| \pm \frac{3}{8} \frac{|\mathbf{q}|^2}{|\Delta_{s\sigma}|}, \quad (6)$$

where $\Delta_{s\sigma} = -UM\sigma - s3\sqrt{3}\lambda$. Thus, the characteristics of low-lying electron quasiparticles can be summarized as (i) the presence of staggered magnetization leads to the asymmetrical energy dispersion of electron quasiparticles, and the direct energy gaps for up- and down-spin electrons are identical, i.e., $2|\Delta_{-1\uparrow}| = 2|\Delta_{+1\downarrow}|$; (ii) in the presence of energy gap $\Delta_{s\sigma}$, the linear-in-momentum energy dispersion of the low-lying electron quasiparticles becomes of the quadratic dependence upon momentum. In this sense, the gradient of $E_{q s \sigma}^{(\pm)}$ with respect to the momentum \mathbf{k} then \mathbf{q} vanishes as \mathbf{k} approaches the Dirac points K and K', indicating a Van Hove singularity, as well as that the low-energy transport properties are dominated by these low-lying electron quasiparticles.

Based on Kubo formula[See Eq.(5)] from the linear response theory⁴³, we study the energy dependence of the longitudinal and traverse optical conductivities of Haldane-Hubbard model in Fig.2(a) and (b), respectively, at $\delta = 0$ and $\lambda = 0.3$ with $U = 4.7$ (black), 4.85(red), 4.9(blue), and 5.0(magenta). The main characteristics of the longitudinal optical conductivity σ_{xx} (solid lines) and σ_{yy} (dashed lines), as well as the traverse optical conductivity σ_{xy} (solid lines) and σ_{yx} (dashed lines) can be summarized as: (i) in the presence of TRS, there is no spin-polarized electrical current even if there exists significant spin splitting in the odd-parity ALMI phase of Haldane-Hubbard model. However if the TRS is broken by external elements such as the sublattice potential, light, or magnetic impurities, the spin current appears [the related work is ongoing, and the results will be presented elsewhere.], which indicates that the odd-parity ALM system with TRS breaking could be a useful platform for the realization of spin currents; (ii) there exists a significant peak in the longitudinal and traverse optical conductivity, $\sigma_L(\Omega)$ and $\sigma_T(\Omega)$, as energy is in the vicinity of the single-particle direct energy gap $2|\Delta_{-1\uparrow}|$, indicating that the optical conductivities are dominated by the low-lying quasiparticle excitations centered around the Dirac points; (iii) the peak location in optical conductivities exhibits a consistent λ and U dependence with the single-particle energy gap which implies that the optical conductivity could be a useful measurement to study the topological phase transition; (iv) the longitudinal optical conductivity displays anisotropic energy dependence at

high energies with $\Omega > 2|\Delta_{-1\uparrow}|$, while after revisiting the longitudinal optical conductivity in the tight-binding model on the honeycomb lattice with vanishing λ and U , we find that this anisotropy survives, which indicates that the anisotropic longitudinal optical conductivities come from the geometry of the honeycomb lattice; (v) as shown in Fig.2(b), the traverse optical conductivities change its sign upon the occurrence of topological phase transition that is consistent with the sign change of the Berry curvature as shown in Fig.2 of the supplemental material.

As shown in Fig.2(b) of the Sup. Mat., when the Haldane-Hubbard model transits from the ALM CI state into the topologically trivial ALMI phase with $C = 0$, there remain substantial negative Berry curvatures in the vicinity of Dirac points K and K', as well as positive ones pervade around the midpoint between them. Therefore, the nonzero anomalous Hall conductivity can be expected when the lower band is partially occupied. Starting from the Berry curvature in Eq.(14) of the supplemental material, the anomalous Hall conductivity⁴⁵ is calculated as

$$\sigma_{\text{Hall}} = -\frac{e^2}{h} \frac{1}{(2\pi)^2} \sum_{\sigma n} \int_{\text{BZ}} d\mathbf{k} B_{\sigma}^{(n)}(\mathbf{k}) n_F(E_{\mathbf{k}\sigma}^{(n)}), \quad (7)$$

where the summation of n is over the occupied energy bands. We in Fig.2(c) study the anomalous Hall conductivity as a function of hole doping δ for $U = 4.8$ and $\lambda = 0.3$ (black), $U = 4.9$ and $\lambda = 0.325$ (red), $U = 5.0$ and $\lambda = 0.35$ (blue), as well as $U = 5.0$ and $\lambda = 0.3$ (magenta), and these parameters have been denoted by blue squares in Fig.1(c). As shown in Fig.2(c), the anomalous Hall conductivity in the ALM CI state first drops dramatically as Haldane-Hubbard model deviates from half-filling, and then decreases gradually with further increment of the hole doping. In addition, as pointed out by the black solid arrow, there exists an inflection point at $\delta \approx 0.2$ and at both sides of this hole doping level, the dependence of the anomalous Hall conductivity upon the Haldane hopping λ is reversed. Moreover, though the anomalous Hall conductivity of the half-filled Haldane-Hubbard model vanishes in the ALMI state, this quantity exhibits a non-monotonous behavior with the growth of hole doping. A similar behavior of the anomalous Hall conductivity has been observed in the interacting modified Kane-Mele model³⁹.

In Fig.2(d), we study the hole doping dependence of the staggered magnetization M [See Eq.(3)] with the same parameters as in Fig.2(c). The main characteristics of this figure can be summarized as (i) compared to the monotonously decreasing M in the ALMI state as shown by the solid line in magenta color that is consistent with the conventional antiferromagnets⁴⁶⁻⁵⁰, the staggered magnetization in the ALM CI phase exhibits a non-monotonous behavior with the increment of hole doping; (ii) there exists an inflection point at $\delta \approx 0.075$, on both sides of which the staggered magnetization displays opposite dependence upon the Haldane hopping strength

λ .

Discussion and conclusion—By adopting the spin group method to analyze the reason why the odd-parity ALM occurs when the nonmagnetic time reversal symmetry is broken, it is shown that compared to the symmetry $[\bar{C}_2||T]$ in the even-parity ALM induced by anisotropic electric crystal potentials, the symmetry connected to the transformation \bar{C}_2 in the spin-only group now changes as: $[\bar{C}_2||\bar{E}]$ or $[\bar{C}_2||\bar{E}t]$, which implies that for odd-parity ALM systems, the single-particle energy dispersion is subjected to the relation $E_{\mathbf{k}\sigma} = E_{-\mathbf{k}-\sigma}$. As a standard example with the presence of sublattice currents, the phase diagram of Haldane-Hubbard model in the λ - U parameter space is reestablished which is composed of three regimes: CI with $C = 2$, ALM CI with $M > 0$ and $C = 2$, and the ALMI with $M > 0$ and $C = 0$. Moreover, we revealed clearly that it is the competition between the staggered magnetization and the alternate magnetic flux in the Haldane model leads to the topological phase transition from the ALM CI state to the ALMI state.

The optical conductivity of Haldane-Hubbard model is further studied using the Kubo formula. The results show that the longitudinal and traverse optical conductivities are not spin-polarized because of the TRS in odd-parity ALM systems, while display a significant peak in the vicinity of the single-particle direct energy gap $2|\Delta_{s\sigma}|$, which reflects a basic fact that both the longitudinal and traverse optical conductivities are dominated by the low-

lying quasiparticle excitations around the Dirac points. The hole doping dependence of the anomalous Hall conductivity σ_{Hall} as well as the staggered magnetization M is also studied. We find that σ_{Hall} in the ALM CI state is diminished monotonically from its initial value $C = 2$ at half-filling as the hole doping is increased, while that in the ALMI state exhibits a non-monotonous behavior that is similar to the interacting modified Kane-Mele model³⁹. However, the staggered magnetization displays an opposite behavior to σ_{Hall} .

ACKNOWLEDGMENTS

This work was supported by the National Key Research and Development Program of China under Grant Nos. 2023YFA1406500 and 2021YFA1401803, the National Natural Science Foundation of China (NSFC) under Grant Nos. 12222402, 92365101, 12474151, 12347101, 12247116, and 12274036, Beijing National Laboratory for Condensed Matter Physics under Grant No. 2024BNLCMPKF025, the Fundamental Research Funds for the Central Universities under Grant No. 2024IAIS-ZX002, the Chongqing Natural Science Foundation under Grants Nos. CSTB2023NSCQ-JQX0024 and CSTB2022NSCQ-MSX0568, and the Special Funding for Postdoctoral Research Projects in Chongqing under Grant No. 2024CQBSHTB3156.

* donghuixu@cqu.edu.cn

† rcwang@cqu.edu.cn

¹ S. López-Moreno, A. H. Romero, J. Mejía-López, A. Muñoz, and I. V. Roshchin, First-principles study of electronic, vibrational, elastic, and magnetic properties of FeF₂ as a function of pressure, *Phys. Rev. B* **85**, 134110 (2012).

² Y. Noda, K. Ohno, and S. Nakamura, Momentum-dependent band spin splitting in semiconducting MnO₂: a density functional calculation, *Phys. Chem. Chem. Phys.* **18**, 13294 (2016).

³ T. Okugawa, K. Ohno, Y. Noda, and S. Nakamura, Weakly spin-dependent band structures of antiferromagnetic perovskite LaMO₃ (M = Cr, Mn, Fe), *J. Phys. Condens. Matter* **30**, 075502 (2018).

⁴ K.-H. Ahn, A. Hariki, K.-W. Lee, and J. Kuneš, Antiferromagnetism in RuO₂ as d -wave Pomeranchuk instability, *Phys. Rev. B* **99**, 184432 (2019).

⁵ S. Hayami, Y. Yanagi, and H. Kusunose, Momentum-Dependent Spin Splitting by Collinear Antiferromagnetic Ordering, *J. Phys. Soc. Jpn.* **88**, 123702 (2019).

⁶ M. Naka, S. Hayami, H. Kusunose, Y. Yanagi, Y. Motome, and H. Seo, Spin current generation in organic antiferromagnets, *Nat. Commun.* **10**, 4305 (2019).

⁷ L. Šmejkal, R. González-Hernández, T. Jungwirth, and J. Sinova, Crystal time-reversal symmetry breaking and spontaneous Hall effect in collinear antiferromagnets, *Sci. Adv.* **6**, eaaz8809 (2020).

⁸ L.-D. Yuan, Z. Wang, J.-W. Luo, E. I. Rashba, and A. Zunger, Giant momentum-dependent spin splitting in centrosymmetric low- Z antiferromagnets, *Phys. Rev. B* **102**, 014422 (2020).

⁹ S. Hayami, Y. Yanagi, and H. Kusunose, Bottom-up design of spin-split and reshaped electronic band structures in antiferromagnets without spin-orbit coupling: Procedure on the basis of augmented multipoles, *Phys. Rev. B* **102**, 144441 (2020).

¹⁰ I. I. Mazin, K. Koepnick, M. D. Johannes, R. González-Hernández, and L. Šmejkal, Prediction of unconventional magnetism in doped FeSb₂, *Proc. Natl. Acad. Sci. U.S.A.* **118**, e2108924118 (2021).

¹¹ L.-D. Yuan, Z. Wang, J.-W. Luo, and A. Zunger, Prediction of low- Z collinear and noncollinear antiferromagnetic compounds having momentum-dependent spin splitting even without spin-orbit coupling, *Phys. Rev. Mater.* **5**, 014409 (2021).

¹² M. Naka, Y. Motome, and H. Seo, Perovskite as a spin current generator, *Phys. Rev. B* **103**, 125114 (2021).

¹³ R. González-Hernández, L. Šmejkal, K. Výborný, Y. Yahagi, J. Sinova, T. c. v. Jungwirth, and J. Železný, Efficient Electrical Spin Splitter Based on Nonrelativistic Collinear Antiferromagnetism, *Phys. Rev. Lett.* **126**, 127701 (2021).

¹⁴ D.-F. Shao, S.-H. Zhang, M. Li, and E. Y. Eom, Chang-Beom and Tsymbal, Spin-neutral currents for spintronics, *Nat. Commun.* **12**, 7061 (2021).

- ¹⁵ L. Šmejkal, A. B. Hellenes, R. González-Hernández, J. Sinova, and T. Jungwirth, Giant and Tunneling Magnetoresistance in Unconventional Collinear Antiferromagnets with Nonrelativistic Spin-Momentum Coupling, *Phys. Rev. X* **12**, 011028 (2022).
- ¹⁶ H. Bai, L. Han, X. Y. Feng, Y. J. Zhou, R. X. Su, Q. Wang, L. Y. Liao, W. X. Zhu, X. Z. Chen, F. Pan, X. L. Fan, and C. Song, Observation of Spin Splitting Torque in a Collinear Antiferromagnet RuO₂, *Phys. Rev. Lett.* **128**, 197202 (2022).
- ¹⁷ A. Bose, N. J. Schreiber, R. Jain, D.-F. Shao, H. P. Nair, J. Sun, X. S. Zhang, D. A. Muller, E. Y. Tsybal, D. G. Schlom, and D. C. Ralph, Tilted spin current generated by the collinear antiferromagnet ruthenium dioxide, *Nat. Electron* **5**, 274 (2022).
- ¹⁸ S. Karube, T. Tanaka, D. Sugawara, N. Kadoguchi, M. Kohda, and J. Nitta, Observation of Spin-Splitter Torque in Collinear Antiferromagnetic RuO₂, *Phys. Rev. Lett.* **129**, 137201 (2022).
- ¹⁹ B. W. F. and E. R. James, Theory of spin-space groups, *Proc. R. Soc. Lond. A* **294**, 343–358 (1966).
- ²⁰ D. Litvin and W. Opechowski, Spin groups, *Physica* **76**, 538 (1974).
- ²¹ D. B. Litvin, Spin point groups, *Acta Crystallogr. Sect. A* **33**, 279 (1977).
- ²² L. Šmejkal, J. Sinova, and T. Jungwirth, Beyond Conventional Ferromagnetism and Antiferromagnetism: A Phase with Nonrelativistic Spin and Crystal Rotation Symmetry, *Phys. Rev. X* **12**, 031042 (2022).
- ²³ L. Šmejkal, J. Sinova, and T. Jungwirth, Emerging Research Landscape of Altermagnetism, *Phys. Rev. X* **12**, 040501 (2022).
- ²⁴ L. Bai, W. Feng, S. Liu, L. Šmejkal, Y. Mokrousov, and Y. Yao, Altermagnetism: Exploring New Frontiers in Magnetism and Spintronics, *Adv. Funct. Mater.* **34**, 2409327 (2024).
- ²⁵ L. Landau and E. Lifshitz, *Electrodynamics of Continuous Media, 2nd ed., Course of Theoretical Physics Vol. 8* (Pergamon Press, Oxford, 1965).
- ²⁶ L. Néel, Magnetism and Local Molecular Field, *Science* **174**, 985 (1971).
- ²⁷ A. Corticelli, R. Moessner, and P. A. McClarty, Spin-space groups and magnon band topology, *Phys. Rev. B* **105**, 064430 (2022).
- ²⁸ E. Turov, *Physical Properties of Magnetically Ordered Crystals* (Academic Press, New York, 1965).
- ²⁹ A. S. Núñez, R. A. Duine, P. Haney, and A. H. MacDonald, Theory of spin torques and giant magnetoresistance in antiferromagnetic metals, *Phys. Rev. B* **73**, 214426 (2006).
- ³⁰ N. J. Ghimire, A. S. Botana, J. S. Jiang, J. Zhang, Y.-S. Chen, and J. F. Mitchell, Large anomalous Hall effect in the chiral-lattice antiferromagnet CoNb₃S₆, *Nat. Commun.* **9**, 3280 (2018).
- ³¹ Y.-P. Lin, Odd-parity altermagnetism through sublattice currents: From haldane-hubbard model to general bipartite lattices, *arXiv:2503.09602* (2025).
- ³² J. He, Y.-H. Zong, S.-P. Kou, Y. Liang, and S. Feng, Topological spin density waves in the Hubbard model on a honeycomb lattice, *Phys. Rev. B* **84**, 035127 (2011).
- ³³ W. Zheng, H. Shen, Z. Wang, and H. Zhai, Magnetic-order-driven topological transition in the Haldane-Hubbard model, *Phys. Rev. B* **91**, 161107 (2015).
- ³⁴ V. S. Arun, R. Sohal, C. Hickey, and A. Paramekanti, Mean field study of the topological Haldane-Hubbard model of spin- $\frac{1}{2}$ fermions, *Phys. Rev. B* **93**, 115110 (2016).
- ³⁵ J. Wu, J. P. L. Faye, D. Sénéchal, and J. Maciejko, Quantum cluster approach to the spinful Haldane-Hubbard model, *Phys. Rev. B* **93**, 075131 (2016).
- ³⁶ T. I. Vanhala, T. Siro, L. Liang, M. Troyer, A. Harju, and P. Törmä, Topological Phase Transitions in the Repulsively Interacting Haldane-Hubbard Model, *Phys. Rev. Lett.* **116**, 225305 (2016).
- ³⁷ J. Imriška, L. Wang, and M. Troyer, First-order topological phase transition of the Haldane-Hubbard model, *Phys. Rev. B* **94**, 035109 (2016).
- ³⁸ W.-X. He, R. Mondaini, H.-G. Luo, X. Wang, and S. Hu, Phase transitions in the Haldane-Hubbard model, *Phys. Rev. B* **109**, 035126 (2024).
- ³⁹ T. Sato, S. Haddad, I. C. Fulga, F. F. Assaad, and J. van den Brink, Altermagnetic Anomalous Hall Effect Emerging from Electronic Correlations, *Phys. Rev. Lett.* **133**, 086503 (2024).
- ⁴⁰ F. D. M. Haldane, Model for a Quantum Hall Effect without Landau Levels: Condensed-Matter Realization of the "Parity Anomaly", *Phys. Rev. Lett.* **61**, 2015 (1988).
- ⁴¹ Q.-H. Wang and D.-H. Lee, Quasiparticle scattering interference in high-temperature superconductors, *Phys. Rev. B* **67**, 020511 (2003).
- ⁴² M. Zeng, X. Li, Y. Wang, and S. Feng, Quasiparticle scattering interference in cuprate superconductors, *Phys. Rev. B* **110**, 134523 (2024).
- ⁴³ G. D. Mahan, *Many-Particle Physics* (Plenum Press, New York, 1990).
- ⁴⁴ Y. Fang, J. Cano, and S. A. A. Ghorashi, Quantum Geometry Induced Nonlinear Transport in Altermagnets, *Phys. Rev. Lett.* **133**, 106701 (2024).
- ⁴⁵ L. Šmejkal, A. H. MacDonald, J. Sinova, S. Nakatsuji, and T. Jungwirth, Anomalous Hall antiferromagnets, *Nat. Rev. Mat.* **7**, 482 (2022).
- ⁴⁶ B. Keimer, S. A. Kivelson, M. R. Norman, S. Uchida, and J. Zaanen, From quantum matter to high-temperature superconductivity in copper oxides, *Nature* **518**, 179 (2015).
- ⁴⁷ T. K. Lee and S. Feng, Doping dependence of antiferromagnetism in La₂CuO₄: A numerical study based on a resonating-valence-bond state, *Phys. Rev. B* **38**, 11809 (1988).
- ⁴⁸ W.-C. Lee and T.-K. Lee, Antiferromagnetism in the Hubbard model using a cluster slave-spin method, *Phys. Rev. B* **96**, 115114 (2017).
- ⁴⁹ M.-H. Zeng, T. Ma, and Y.-J. Wang, Phase diagram of the Hubbard model on a square lattice: A cluster slave-spin study, *Phys. Rev. B* **104**, 094524 (2021).
- ⁵⁰ M.-H. Zeng, Y.-J. Wang, and T. Ma, Phase diagram of the Hubbard model on a honeycomb lattice: A cluster slave-spin study, *Phys. Rev. B* **105**, 035155 (2022).